First-principles perspective on full-spectrum infrared photodetectors from doping an excitonic insulator

Jing Liu and Yuanchang Li[*]

Key Laboratory of Advanced Optoelectronic Quantum Architecture and Measurement (MOE), Beijing 100081, China
and Advanced Research Institute of Multidisciplinary Science, Beijing Institute of Technology, Beijing 100081, China

Innovations in imaging technology involve finding strategies and materials suitable for detection applications over the entire infrared range. Herein, we propose a new design concept based on the unique feature of an excitonic insulator, namely, negative exciton transition energy (E_t). We demonstrate this concept using first-principles GW-Bethe-Salpeter equation calculations on one-dimensional organometallic wire $(CrBz)_\infty$. The pristine $(CrBz)_\infty$ exhibits an excitonic instability due to a negative E_t for the lowest exciton. Substitutional doping can continuously tune the E_t from ~ 0 to ~ 0.6 eV, which shows the ability of photon detection from terahertz to near infrared. This type of detector has advantages of outstanding wavelength selectivity, reduced thermal disturbance, and elevated working temperature. Our paper not only adds another member in the family of rare one-dimensional excitonic insulators, but also opens a new avenue for the development of high-performance infrared photodetectors in the future.

I. INTRODUCTION

Infrared photon detection is of utmost importance for a wide range of applications, including night vision, bioimaging, communications, remote sensing, environmental monitoring, security checking, radio astronomy, etc. [1–7]. Present-day photodetectors rely primarily on the semiconductors' band gap which determines the minimum photon energy to convert into electrical signals for subsequent processing. As a result, narrow gap systems are chosen to fabricate high-performance infrared detectors. The $Hg_{1-x}Cd_xTe$ alloy is nowadays the leading compound for applications over almost the entire infrared range from short (1–3-μm) to very long (14–30-μm) wavelength (corresponding to the photon energy of 0.04–1.24 eV), ascribed to its continuously adjustable band gap from negative of HgTe to positive of CdTe with the increase in x [1,2]. Nevertheless, $Hg_{1-x}Cd_xTe$ is restrained by some fundamental limitations including high manufacturing costs, a complicated synthetic process, cryogenic operating environment, precise composition control, in addition to material toxicity [1,5–7]. There has been an ever-increasing demand for finding new design concepts and/or alternative versatile materials that can compete with and eventually replace $Hg_{1-x}Cd_xTe$ technologies. For this purpose, a photoresponse in the whole infrared band is a prerequisite. Emerging gapless materials, such as graphene and topological semimetals are, thus, demonstrated for ultrabroadband photon detection, but the performance is substantially hampered by low overall quantum efficiency and high dark current [7,8].

In reality, the material's optical response must involve excitons (bound electron-hole pairs by Coulomb interaction) because excitons are first created from light harvesting, and their subsequent charge separation produces current. The excitons are often ignored due to their small binding energy in traditional narrow-gap semiconductors, in which the excitons, once formed, would readily dissociate via thermal activation [9,10]. Instead, if the exciton effect is sufficiently significant, photodetectors can be fully designed based on the exciton [11].

The excitonic insulator, proposed some half century ago, has a many-body ground state characterized by spontaneously formed exciton condensate [12]. It is viewed as an analog to the BCS superconductor and expected to host amazing macroscopic quantum properties, such as supertransport [13–15]. Although, to date, there is no universally accepted excitonic insulator, recent advances in low-dimensional materials have opened new avenues for the search and the discovery of such insulators [16–23]. The excitonic insulator emerges when the exciton binding energy (E_b) exceeds the one-electron band-gap (E_g), so the lowest characteristic exciton has an inherently negative transition energy ($E_t = E_g - E_b$) [12]. With this unique property, the excitonic insulators offer an unprecedented opportunity for exciton-based full-spectrum infrared detection because they hold the potential to allow continuous regulation of E_t from negative to positive, just as continuous regulation of E_g in $Hg_{1-x}Cd_xTe$ alloys. This is unusual as a gapped system generally presents a positive E_t, which defines the longest wavelength of detection. In this light, the excitonic insulators are among the most attractive alternatives to replace $Hg_{1-x}Cd_xTe$ for the infrared detection. It has to be noted, however, that the characteristic exciton in an excitonic insulator is optically inactive [23–25], and, therefore, stimulating its optical activity represents another necessary prerequisite for the realization of excitonic-insulator infrared detection.

In this paper, through first-principles GW plus Bethe-Salpeter equation (BSE) calculations, we illustrate the strategy of designing exciton-based full-spectrum infrared
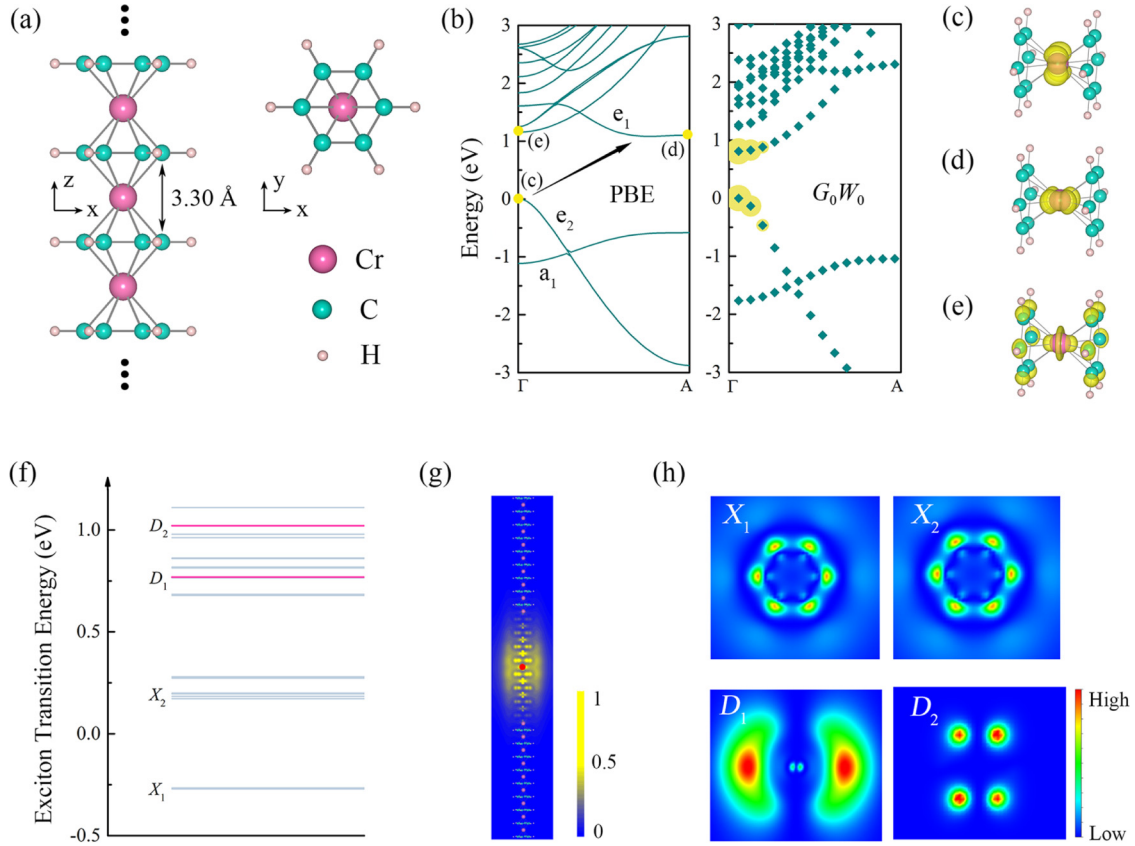
*yuancli@bit.edu.cn

FIG. 1. (a) Crystal structure of the $(CrBz)_\infty$ wire. (b) PBE (left) and G_0W_0 (right) band structures with the valence-band maximum as energy zero. The minimum PBE gap is denoted by the arrow in the left panel. The yellow dots superimposed on the GW band indicate the BSE fatband structure to visually inspect **k**-dependent contribution of electron-hole pairs to the lowest X_1 exciton. The larger the yellow dot, the larger the contribution. See the main text for details. (c)–(e) Decomposed charge densities for the states marked in (b) (yellow dots) with an isosurface of 0.02, 0.02 and 0.003 $e/\text{Å}^3$. (f) Transition energies of low-energy excitons for the $(CrBz)_\infty$ wire, where D and X series represent the bright (pink lines) and dark (gray lines) excitons, respectively. (g) Side view of the real-space exciton wave functions for the X_1, whose modulus is truncated at 50% of the maximum to specify the details. A $1 \times 1 \times 25$ supercell is used for calculations and the hole (red dot) is fixed at the central Cr atom. (h) Cross sections of the real-space exciton wave functions cutting through the Bz ring for the states marked in (f).

detector by substitutionally doping an excitonic insulator. First, we show the occurrence of excitonic instability in one-dimensional organometallic sandwich chromium-benzene (Bz) wire $(CrBz)_\infty$, whose characteristic exciton has a negative E_t of -0.27 eV and a giant E_b up to 1.08 eV. Then we investigate the effect of substitutional doping (H → F and C → N) on the characteristic exciton. We find a gradual blueshift of E_t from negative to around zero, and to positive, depending on the dopant concentration and distribution, whereas maintaining $E_b > 0.5$ eV. Moreover, the doping causes symmetry breaking and accordingly, the characteristic exciton is optically activated. All these together indicate the feasibility of building an exciton-based full-spectrum infrared detector that can work at high temperature. Finally, we discuss the advantages of here studied exciton-based detectors over traditional band-gap-based ones in terms of color selectivity and reduced thermal disturbance.

II. METHODOLOGY AND MODELS

All DFT calculations were performed using the Vienna *ab initio* simulation package (VASP) [26] within the Perdew-Burke-Ernzerhof (PBE) exchange-correlation functional [27].

The projector augmented-wave [28] method was used with a cutoff kinetic energy of 500 eV. A supercell model was adopted for the isolated $(CrBz)_\infty$ and the separation between two neighboring wires was, at least, 12 Å (see the Supplemental Material [29] for convergence studies). Single-shot G_0W_0 calculations were carried out for the quasiparticle band structure [30] with a k-mesh density no less than $14/\text{Å}$ and a total of more than six times the number of valence bands. The BSE is solved for excitonic properties [31] on top of the G_0W_0 results with three valence and four conduction bands included for the BSE Hamiltonian. Exciton wave functions were obtained from the YAMBO code [32].

III. RESULTS AND DISCUSSION

A one-dimensional $(CrBz)_\infty$ wire consists of alternately arranged Cr atoms and Bz rings as plotted in Fig. 1(a). Its ground-state structure possesses the D_{6h} symmetry [33]. Under such a crystal field, the Cr $3d$ orbitals split into e_1 (d_{xz} and d_{yz} orbitals) and e_2 ($d_{x^2-y^2}$ and d_{xy} orbitals) doublets, and a_1 (d_{z^2} orbital) singlet [34,35]. The six valence electrons of Cr completely occupy the lower-lying a_1 singlet and e_2 doublet, leaving the e_1 doublet unoccupied. So $(CrBz)_\infty$ is

TABLE I. The G_0W_0 gap E_g (eV), the exciton transition energy E_t (eV), and the exciton binding energy E_b (eV), corresponding to the different crystal structures inserted in Fig. 2.

	CrC_5NH_5	$(CrC_5NH_5)_2^d$	$(CrC_5NH_5)_2^s$	$Cr_2C_{11}NH_{11}$	$Cr_2C_{11}NH_{10}F$	$CrC_6H_4F_2$	$CrC_6H_3F_3$
E_g	0.945	1.010	0.995	0.832	1.108	1.497	1.780
E_t	0.060	0.123	0.207	0.326	0.417	0.529	0.627
E_b	0.885	0.887	0.789	0.506	0.691	0.968	1.153

expected to be a non-spin-polarized semiconductor with an e_1 and e_2 doublet separated gap. Our PBE calculations verify this picture and give an indirect gap of 1.08 eV as shown by the arrow in the left panel of Fig. 1(b). But this is contrast to a previous report of a direct gap 0.71 eV at Γ using the PW91 functional [33]. Our high-level theoretical calculations by the GW yields a direct gap of 0.81 eV at Γ [see the right panel of Fig. 1(b)].

Such an indirect-direct gap transition is a manifestation of orbital-dependent quasiparticle corrections, a well-known feature of GW [36–38]. To illustrate this, we plot decomposed charge densities for the states marked in the left panel of Fig. 1(b). It can be seen that the states labeled as (c) and (d) in Fig. 1(b) are mainly contributed by the localized Cr d orbitals whereas the state labeled as (e) in Fig. 1(b) is by the Bz delocalized π orbitals. Because of their different delocalization errors by PBE, the quasiparticle corrections for the d orbitals are generally much larger than those for the π orbitals. As a result, both e_1 and e_2 bands with more localized d character are pushed up considerably with respect to the Bz π band. Specifically, the calculated quasiparticle corrections for states shown in Figs. 1(c), 1(d) and 1(e) are 0.94, 2.19, and 0.63 eV, respectively. Thus, when we align the e_2 valence-band maximum of PBE and GW uniformly to energy zero, it looks like an unusual "downshift" of 0.31 eV in the π band by GW. In order to be certain of our findings, we also compare the band structures of G_0W_0 by YAMBO and of the HSE06 by VASP in Fig. S2 in the Supplemental Material [29]. They all show the same direct-gap feature.

We then solve the BSE for the excitonic properties and the E_t of low-energy excitons are summarized in Fig. 1(f). Herein both bright and dark excitons are considered (denoted as D and X series, respectively). The most interesting finding is a negative E_t, namely, -0.27 eV for the lowest X_1 exciton, which means its spontaneous formation and the occurrence of excitonic instability. Therefore, $(CrBz)_\infty$ can serve as a rare candidate for an intrinsic one-dimensional excitonic insulator. To our knowledge, carbon nanotubes are the only intrinsically one-dimensional excitonic insulators reported [18]. Nevertheless, there is a clear difference between carbon nanotubes and $(CrBz)_\infty$ in that excitonic instabilities occur in a near-zero band-gap system and a finite band-gap (0.81-eV) semiconductor, respectively.

Despite this difference, the large E_b of both carbon nanotubes and $(CrBz)_\infty$ should come from the weakening of the electron-hole screening effect due to the dimensionality reduction. To learn more about the lowest X_1 exciton, we use fatband picture to visually inspect which electron-hole pairs in **k** space contribute the most to its eigenstate [21]. As can be clearly seen in the right panel of Fig. 1(b), the band-edge states near the Γ point contribute the most. Relative

localization around the Brillouin-zone center in the reciprocal space makes the X_1 exciton Wannier-Mott-like. Whereas in Fig. 1(g), we show its wave functions in the real space. It is also highly localized and distributed within only a few unit cells, behaving like a Frenkel exciton. These illustrate the unique characteristics of one-dimensional excitons.

In practice, only the bright excitons have optical response and are useful for light absorption and detection whereas the dark excitons are not. However, the characteristic exciton that leads to instability in excitonic insulators is generally dark [23,25], such as here the X_1. This apparent contradiction has to be solved before realizing the photon detection based on the excitonic insulators. According to the knowledge of group theory, optical inactivity of the X_1 is resulted from the dipole forbidden transition between band-edge states in terms of the unique D_{6h} symmetry of the $(CrBz)_\infty$. To illustrate this point more clearly, we representatively select two excitons from the D and X series, respectively, and compare their characteristics in Fig. 1(h). It is obviously seen that the X-series excitons all respect the D_{6h} symmetry whereas the D-series excitons show different degrees of symmetry breaking.

A full-spectrum exciton-based infrared detector involves three key elements of the characteristic exciton: continuously adjustable E_t almost from zero, large enough E_b and optical activity. Herein, we focus on the means of substitutional doping, including the replacement of C(H) with N(F) for the following four considerations: (1) Such reactions have been chemically established and result in small structural changes [39,40], (2) it is able to modulate the materials' electronic and optical properties effectively [41], (3) it can yield symmetry breaking, hence, causing dark-to-bright exciton conversion, and (4) it affects E_b relatively marginally [22]. The calculated results of several representative substitutions are presented in Table I and Fig. 2. Indeed, the doping tunes E_t of the characteristic exciton, ranging from ~ 0 eV to ~ 0.6 eV in terms of different dopants, concentrations, and distributions, whereas keeping the $E_b > 0.5$ eV (see Table I). The clear absorption peak related to the characteristic exciton has also been observed from the imaginary part of the BSE dielectric function (see Fig. 2). Combination of these three central points indicates the promising application potential for full-spectrum infrared detection, which can even extend to the terahertz band and work at room temperature as well.

Specifically, one N replacing one C gives an E_t of 0.060 eV, very close to zero, which illustrates the possibility for the very far-infrared (~ 20 μm). No novel transitions are introduced by the dopant, and the characteristic excitons are still mainly associated with transitions between the Cr d orbitals and the Bz π orbitals (see Fig. S3 in the Supplemental Material [29]). Maintaining N concentration, the E_t could increase to 0.123 or 0.207 eV depending on whether the two N atoms are in
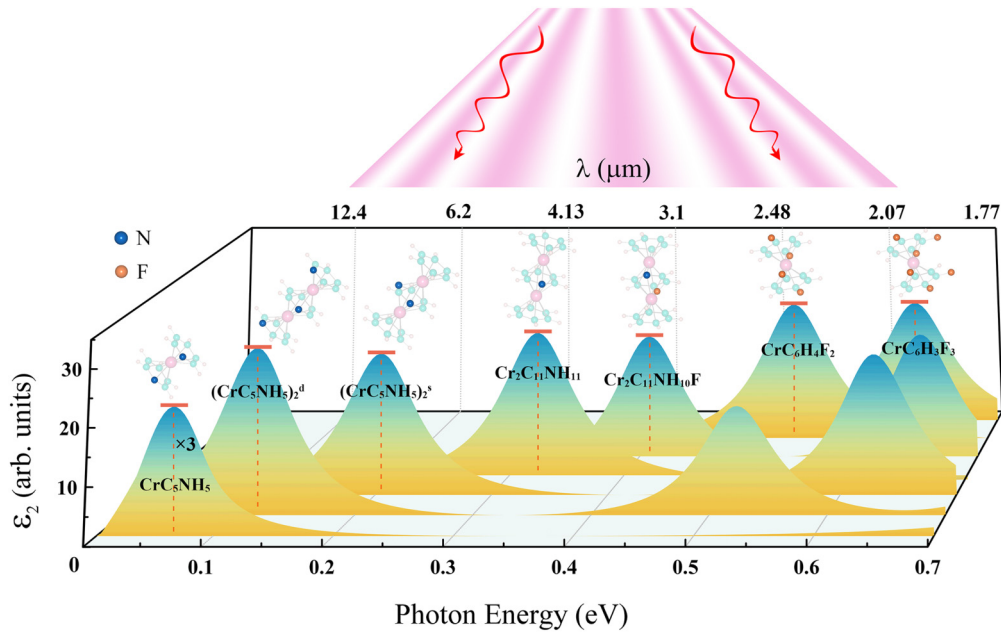
FIG. 2. The calculated imaginary part of the BSE dielectric function for different doping systems with the incident light perpendicular to the wire. See Table I for more details. For clarity, the intensity of CrC_5NH_5 is multiplied by three. The insets show the crystal structures of doped $(CrBz)_\infty$.

different or the same Bz. Halving N concentration further increases the E_t to 0.326 eV. On the other hand, F replacing H tends to cause the blueshift of both E_t and E_g (see Table I). It is worth noting that, shown here are only a few concrete examples, but in principle, any E_t between zero and electronic band gap can be obtained via appropriate doping. This fact supports our statement of an exciton-based full-spectrum photon detection.

The exciton-based infrared detectors have two prominent advantages over traditional band-gap-based ones. One is outstanding wavelength selectivity. As illustrated in Fig. 3(a), exciton absorption refers to discrete energy levels below the electronic band gap and is limited to a very narrow band range. It is, thus, possible to design a photodetector that only

responds to a specific wavelength. This becomes even more practical when assembling with low-dimensional materials where the lowest exciton can be hundreds of millielectron volts away from electronic band gap [24]. In sharp contrast, traditional photodetectors respond to any wavelength light in energy larger than the band gap.

The other is a reduction of the thermal disturbance. The current signal of photodetectors is produced through the charge separation of photoexcited electron-hole pairs under a built-in electric field [42]. Actually, the electron-hole pairs may also be thermally triggered, leading to an electrical output in the absence of light (dark current) and reducing the detection sensitivity. As the detection moving to very far-infrared region, thermal noise would become more
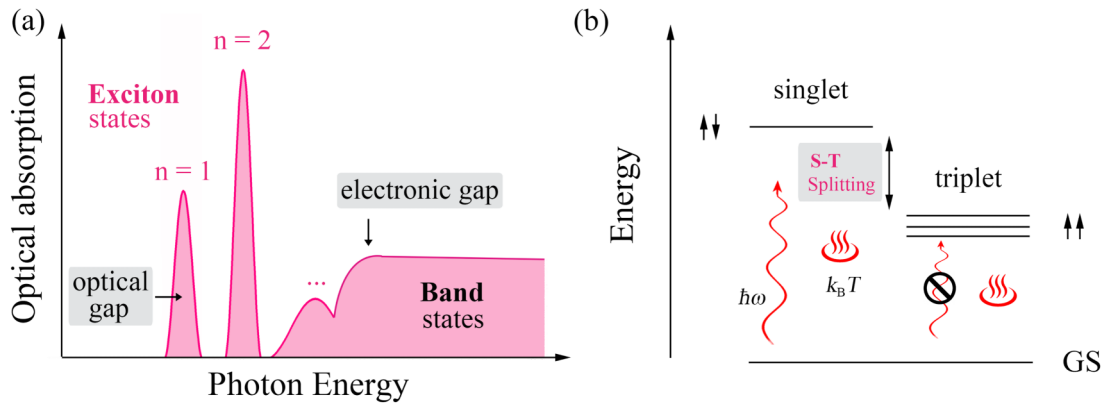

FIG. 3. (a) Typical adsorption spectrum for a low-dimensional system in which the discrete exciton states lie below the electronic band gap and the continuous band states lie above. Energy difference between the electronic band gap and the optical gap defines the E_b of the lowest characteristic exciton. (b) Schematic of the singlet-triplet splitting in terms of exciton spin, and their different optical ($\hbar\omega$) and thermal ($k_B T$) excitations.
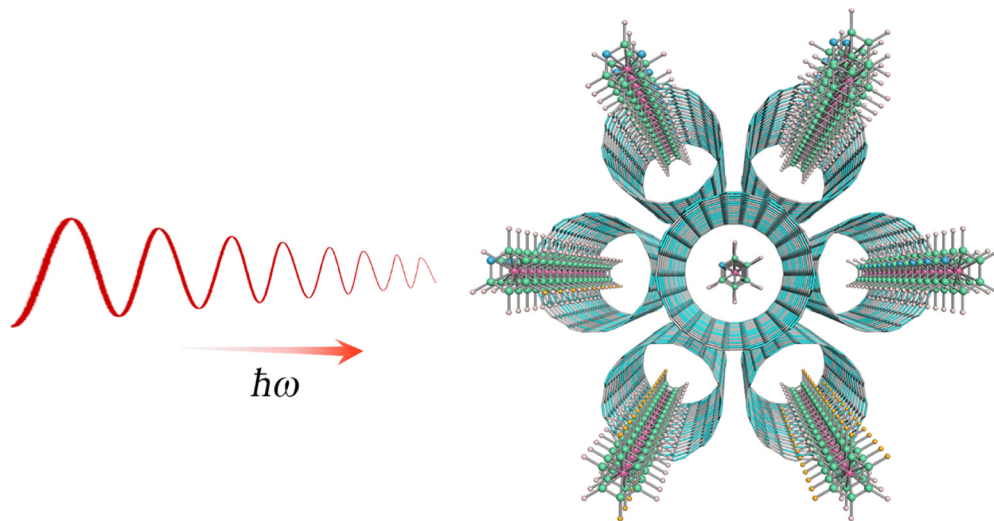
FIG. 4. A device design scheme for full-spectrum infrared detectors based on the array composed of boron nitride nanotube encapsulated doped $(CrBz)_\infty$. Each doped $(CrBz)_\infty$ works as an independent elementary component to detect a specific wavelength. Boron nitride nanotubes are used to reduce the influence on the exciton.

pronounced and might confuse the recognition. Regarding to the band-gap-based paradigm, the longer the target wavelength is, the narrower the band gap is required and the larger the corresponding dark current will be. For example, this poses an almost insurmountable constraint for gapless semimetals, such as graphene and less efficient unbiased mode has to be invoked for the charge separation [7,43].

By contrast, the exciton-based paradigm no longer necessitates a narrow band gap, which would allow the thermal excitation only relevant to occupation of the exciton state rather than the band state. Hence, the dark current could be considerably reduced in exciton-based detectors as compared to their band-gap-based counterparts. In addition, as illustrated in Fig. 3(b), considering spin degree of freedom, the excitons split into a lower-lying triplet and a higher-lying singlet with a small splitting energy. Photoexcitation is only effective for the singlet as a result of the spin-selection rule [21] whereas thermal excitation is effective for both. Such spin-dependent behavior would still provide us with the possibility to extract weak light signals by resolving spin information even if the thermal fluctuation noise overwhelms the photocurrent.

Next we briefly discuss two concerns regarding the practical feasibility. One is related to the fabrication of one-dimensional linear sandwich wires. As far as we know, the $(CrBz)_\infty$ has not been synthesized and no multidecker Cr_nBz_{n+1} clusters other than $CrBz_2$ has been produced [44]. Nevertheless, recent advances in organometallic chemistry have allowed the growth of several of this kind of molecular wires with total metal atoms ranging from a few to a thousand [45–48], and more importantly, the developing method is believed to work for variation of either the ligand (e.g., benzene) or the metal centers (element of the $3d$ or $4f$ series) [47]. In this context, the preparation of $(CrBz)_\infty$ does not seem impossible, and we expect our paper to stimulate experimental interests.

The other concern is related to the environment effect in practical applications, which is of particular importance for the excitonic properties of a one-dimensional system. To this end, we design a working scheme as schematically shown in Fig. 4. Each doped $(CrBz)_\infty$ is encapsulated in a boron nitride nanotube to form an elementary device that only responds to a specific infrared wavelength. Then a large number of such components for different wavelengths are assembled to constitute an infrared detection array. In this way, both the detection bandwidth and the wavelength selectivity can be achieved. Using boron nitride nanotubes is mainly because of its large band gap ($\sim$5 eV), low dielectric-constant, and free of dangling bonds or surface charge traps [21,49]. Not only does this help to eliminate the interwire coupling, hence, maintaining the wavelength selectivity of each elementary device, but the essence of a low dielectric constant also helps to reduce the effect on excitons [21].

IV. CONCLUSIONS

In conclusion, we propose a different design concept for full-spectrum infrared detection by manipulating the characteristic exciton of an excitonic insulator, and its feasibility is verified by the first-principles GW-BSE calculations on the prototype $(CrBz)_\infty$. Unlike the traditional infrared detector, the exciton-based paradigm works by the resonant light absorption of discrete exciton states and, therefore, is much superior in wavelength selectivity. In addition, it can also possess the advantages of high operating temperature and reduced thermal disturbance, going beyond the classical band-gap-based one. Our work not only adds another member in the family of rare one-dimensional excitonic insulators, but also opens an avenue for the development of high-performance infrared photodetectors in the future.

ACKNOWLEDGMENTS

[1] A. Rogalski, Rep. Prog. Phys. **68**, 2267 (2005).

[2] P. Martyniuk, J. Antoszewski, M. Martyniuk, L. Faraone, and A. Rogalski, Appl. Phys. Rev. **1**, 041102 (2014)

[3] Z. Q. Guo, S. Park, J. Yoon, and I. Shin, Chem. Soc. Rev. **43**, 16 (2014).

[4] C. Downs and T. E. Vandervelde, Sensors **13**, 5054 (2013).

[5] D. L. Smith and C. Mailhiot, J. Appl. Phys. **62**, 2545 (1987)

[6] P. Norton, Opto-Electron. Rev. **10**, 159 (2002).

[7] J. Liu, F. N. Xia, D. Xiao, F. Javier García de Abajo, and D. Sun, Nature Mater. **19**, 830 (2020).

[8] F. N. Xia, T. Mueller, Y. M. Lin, A. Valdes-Garcia, and P. Avouris, Nat. Nanotechnol. **4**, 839 (2009).

[9] R. C. Iotti and L. C. Andreani, Semicond. Sci. Technol. **10**, 1561 (1995).

[10] A. Zrenner, P. Leeb, J. Schäfer, G. Böhm, G. Weimann, J. M. Warlock, L. T. Florez, and J. P. Harbison, Surf. Sci. **263**, 496 (1992).

[11] S. Lukman, L. Ding, L. Xu, Y. Tao, A. C. Riis-Jensen, G. Zhang, Q. Y. S. Wu, M. Yang, S. Luo, C. H. Hsu, L. Z. Yao, G. Liang, H. Lin, Y.-W. Zhang, K. S. Thygesen, Q. J. Wang, Y. P. Feng, and J. H. Teng, Nat. Nanotechnol. **15**, 675 (2020).

[12] D. Jérome, T. M. Rice, and W. Kohn, Phys. Rev. **158**, 462 (1967).

[13] J. P. Eisenstein and A. H. MacDonald, Nature (London) **432**, 691 (2004).

[14] A. N. Kozlov and L. A. Maksimov, Zh. Eksperim. i Teor. Fiz. **50**, 131 (1966) [Soviet Phys.-JETP **23**, 88 (1966)].

[15] Q. F. Sun, Z. T. Jiang, Y. Yu, and X. C. Xie, Phys. Rev. B **84**, 214501 (2011).

[16] D. Varsano, M. Palummo, E. Molinari, and M. Rontani, Nat. Nanotechnol. **15**, 367 (2020).

[17] L. J. Du, X. W. Li, W. K. Lou, G. Sullivan, K. Chang, J. Kono, and R. R. Du, Nat. Commun. **8**, 1971 (2017).

[18] D. Varsano, S. Sorella, D. Sangalli, M. Barborini, S. Corni, E. Molinari, and M. Rontani, Nat. Commun. **8**, 1461 (2017).

[19] G. Sethi, Y. N. Zhou, L. H. Zhu, L. Yang, and F. Liu, Phys. Rev. Lett. **126**, 196403 (2021).

[20] Z. Y. Jiang, Y. C. Li, W. H. Duan, and S. B. Zhang, Phys. Rev. Lett. **122**, 236402 (2019).

[21] Z. Y. Jiang, W. K. Lou, Y. Liu, Y. C. Li, H. F. Song, K. Chang, W. H. Duan, and S. B. Zhang, Phys. Rev. Lett. **124**, 166401 (2020).

[22] S. Dong and Y. C. Li, Phys. Rev. B **102**, 155119 (2020).

[23] Z. Jiang, Y. C. Li, S. B. Zhang, and W. H. Duan, Phys. Rev. B **98**, 081408(R) (2018).

[24] Z. Y. Jiang, Z. R. Liu, Y. C. Li, and W. H. Duan, Phys. Rev. Lett. **118**, 266401 (2017).

[25] B. I. Halperin and T. M. Rice, Rev. Mod. Phys. **40**, 755 (1968).

[26] G. Kresse and J. Furthmüller, Phys. Rev. B **54**, 11169 (1996).

[27] J. P. Perdew, K. Burke, and M. Ernzerhof, Phys. Rev. Lett. **77**, 3865 (1996).

[28] P. E. Blöchl, Phys. Rev. B **50**, 17953 (1994); G. Kresse and D. Joubert, *ibid.* **59**, 1758 (1999).

[29] See Supplemental Material at http://link.aps.org/supplemental/10.1103/PhysRevB.106.035135 for convergence studies on the number of k points, vacuum layer, band comparison of different codes and methods for the $(CrBz)_\infty$, and excitonic properties in the $(CrC_5NH_5)_\infty$.

[30] M. S. Hybertsen and S. G. Louie, Phys. Rev. B **34**, 5390 (1986).

[31] M. Rohlfing and S. G. Louie, Phys. Rev. B **62**, 4927 (2000).

[32] A. Marini, C. Hogan, M. Grüning, and D. Varsano, Comput. Phys. Commun. **180**, 1392 (2009).

[33] H. J. Xiang, J. L. Yang, J. G. Hou, and Q. S. Zhu, J. Am. Chem. Soc. **128**, 2310 (2006).

[34] Y. C. Li, G. Zhou, J. Li, J. Wu, B.-L. Gu, and W. H. Duan, J. Phys. Chem. C **115**, 7292 (2011).

[35] Y. C. Li, G. Zhou, J. Wu, and W. H. Duan, J. Chem. Phys. **135**, 014702 (2011).

[36] J. Liu, G.-B. Liu, and Y. C. Li, Phys. Rev. B **104**, 085150 (2021).

[37] L. Yang, M. L. Cohen, and S. G. Louie, Nano Lett. **7**, 3112 (2007).

[38] D. Prezzi, D. Varsano, A. Ruini, A. Marini, and E. Molinari, Phys. Rev. B **77**, 041404(R) (2008).

[39] P. Adler, C. J. Teskey, D. Kaiser, M. Holy, H. H. Sitte, and N. Maulide, Nat. Chem. **11**, 329 (2019).

[40] L. Zhi, T. Gorelik, R. Friedlein, J. Wu, U. Kolb, W. R. Salaneck, and K. Müllen, Small **1**, 798 (2005).

[41] H. Lu, T. Nakamuro, K. Yamashita, H. Yanagisawa, O. Nureki, M. Kikkawa, H. Gao, J. Tian, R. Shang, and E. Nakamura, J. Am. Chem. Soc. **142**, 18990 (2020).

[42] J. Liu, Y. Zhang, J. Chen, R. Bao, K. Jiang, F. Khan, A. Goswami, Z. Li, F. Liu, K. Feng, J. Luo, and T. Thundat, Matter **1**, 650 (2019).

[43] N. Youngblood, C. Chen, S. J. Koester, and M. Li, Nat. Photonics **9**, 247 (2015).

[44] T. Kurikawa, H. Takeda, M. Hirano, K. Judai, T. Arita, S. Nagao, A. Nakajima, and K. Kaya, Organometallics **18**, 1430 (1999).

[45] S. Nagao, A. Kato, A. Nakajima, and K. Kaya, J. Am. Chem. Soc. **122**, 4221 (2000).

[46] K. Miyajima, S. Yabushita, M. B. Knickelbein, and A. Nakajima, J. Am. Chem. Soc. **129**, 8473 (2007).

[47] F. Huttmann, N. Schleheck, N. Atodiresei, and T. Michely, J. Am. Chem. Soc. **139**, 9895 (2017).

[48] V. M. Santhini, O. Stetsovych, M. Ondráček, J. I. Mendieta Moreno, P. Mutombo, B. de la Torre, M. Švec, J. Klívar, I. G. Stará, H. Vázquez, I. Starý, and P. Jelínek, Adv. Funct. Mater. **31**, 2006391 (2020).

[49] C. Dean, A. Young, I. Meric, C. Lee, L. Wang, S. Sorgenfrei, K. Watanabe, T. Taniguchi, P. Kim, K. Shepard, and J. Hone, Nat. Nanotechnol. **5**, 722 (2010).